Published in final edited form as:
Environ Res Lett. ; 7(4): . doi:10.1088/1748-9326/7/4/044034.

Response of air stagnation frequency to anthropogenically enhanced radiative forcing

Daniel E. Horton[1,*], **Harshvardhan**[2], and **Noah S. Diffenbaugh**[1,3]

[1]Department of Environmental Earth System Science, Stanford University, Stanford, CA, USA

[2]Department of Earth & Atmospheric Sciences, Purdue University, West Lafayette, IN, USA

[3]Woods Institute for the Environment, Stanford University, Stanford, CA, USA

Abstract

Stagnant atmospheric conditions can lead to hazardous air quality by allowing ozone and particulate matter to accumulate and persist in the near-surface environment. By changing atmospheric circulation and precipitation patterns, global warming could alter the meteorological factors that regulate air stagnation frequency. We analyze the response of the National Climatic Data Center (NCDC) Air Stagnation Index (ASI) to anthropogenically enhanced radiative forcing using global climate model projections of late-21st century climate change (SRES A1B scenario). Our results indicate that the atmospheric conditions over the highly populated, highly industrialized regions of the eastern United States, Mediterranean Europe, and eastern China are particularly sensitive to global warming, with the occurrence of stagnant conditions projected to increase 12-to-25% relative to late-20th century stagnation frequencies (3-18+ days/year). Changes in the position/strength of the polar jet, in the occurrence of light surface winds, and in the number of precipitation-free days all contribute to more frequent late-21st century air mass stagnation over these high-population regions. In addition, we find substantial inter-model spread in the simulated response of stagnation conditions over some regions using either native or bias corrected global climate model simulations, suggesting that changes in the atmospheric circulation and/or the distribution of precipitation represent important sources of uncertainty in the response of air quality to global warming.

Keywords

air quality; pollution; stagnation; climate change; meteorology; health impacts

1. Introduction

Despite Clean Air legislation in many countries, poor air quality remains a formidable socio-economic burden. Methods used to quantify the economic, environmental, and health impacts of degraded air quality vary, but estimated annual costs are substantial [1-3]. Given the far-reaching and deleterious consequences of degraded air quality, agencies in many nations provide real-time observations and short-term forecasts of near-surface air quality conditions [e.g., 4,5]. These agencies monitor factors that influence air quality, including atmospheric chemistry, particulate matter concentrations, and local weather conditions. Due to uncertainties inherent in the prediction of these factors, particularly in a changing climate system, the generation of long-term air quality projections poses a more difficult challenge, but remains essential to the creation of effective Clean Air regulatory policy [e.g., 6-8].

[*]corresponding author: danethan@stanford.edu.

Research suggests that poor air quality is the result of atmospheric pollutants – primarily particulate matter and tropospheric ozone (and its precursors) – and the meteorological conditions that support their formation and/or accumulation within the near-surface atmosphere [cf. 9]. Accurate long-term projections of air quality require knowledge of future emissions of pollutants, future changes in climate, and the direct and indirect interactions between the two. Our focus in the current study is on uncertainties associated with the response of atmospheric conditions to enhanced radiative forcing. Previous efforts to quantify the effects of anthropogenically enhanced radiative forcing on the atmospheric conditions that influence air quality have used numerical experiments with a limited number of models/realizations [e.g., 10-15]. The lack of multi-model analysis is an important limitation, as air quality projection uncertainties are derived from complicated meteorological dependencies [9] and are therefore subject to a number of potential sources of uncertainty, including the ability of models to accurately simulate the atmospheric processes associated with air quality ("model bias") [10] and the range of projected climatic changes simulated by various models ("inter-model spread") [16].

Studies attempting to isolate the meteorological factors that produce poor air quality have demonstrated that different pollutants and the precursors of those pollutants have different meteorological dependencies, and that these dependencies are further complicated by seasonal and regional variations [e.g., 10-12,17]. In a review of the influence of a suite of meteorological variables on air quality, Jacob and Winner [9] identified atmospheric air stagnation as the only meteorological metric with which both ozone and particulate matter concentrations consistently demonstrated a strong positive correlation. Given this consistent correlation, we attempt to constrain the response of atmospheric air stagnation to elevated greenhouse forcing.

Air stagnation is characterized by meteorological conditions that lack contaminant-scavenging capabilities and minimize the horizontal dispersion and vertical escape of pollutants [18,19]. In the United States, air stagnation is monitored by the National Climatic Data Center (NCDC) via the Air Stagnation Index (ASI), a metric that tracks the monthly frequency of meteorological conditions conducive to air mass stagnation [20]. In the NCDC metric, stagnation events are defined as periods with (*i*) light low level winds, indicative of a stable lower atmosphere with reduced horizontal dispersion and limited vertical escape, (*ii*) light upper level winds, generally associated with the establishment of persistent/slow moving warm core high pressure systems, and (*iii*) a lack of precipitation, minimizing the scavenging of airborne particulate matter.

The ASI has previously been used to demonstrate the relationship between observed 20th century air mass stagnation and elevated particulate matter and surface-level ozone concentrations over the continental U.S. [12,15], and to explore the effects of mid-21st century climate change on continental U.S. air stagnation frequency in a single nested climate model simulation driven by native General Circulation Model (GCM) meteorological fields [10]. Similarly, GCM-driven chemical transport models have been used to investigate the effects of future climate change on air quality and have found that changes in the occurrence of stagnation episodes plays an important role in future air quality projections [13,14]. We build on these studies by employing the multi-GCM CMIP3 ensemble to quantify the uncertainty in the response of the ASI to global warming [16]. We quantify the relative change in air stagnation frequency using daily atmospheric data from the late-20th (20C3M; 1981-2000) and late-21st century (SRESA1B; 2081-2100) simulations from 16 CMIP3 GCMs (Table S1). We bias correct each CMIP3 simulation with atmospheric fields from the NCEP/DOE Reanalysis 2 (R2) [21] and Matsuura and Willmott [22] datasets using the bias correction methodology of Ashfaq et al [23,24].

The design and execution of this study have three primary motivations:

A. The ASI utilized by the NCDC is an objective measure of synoptic-scale stagnation, but its application has thus far been limited to the continental U.S. [19]. We analyze the ASI metric over the global domain, with the intention of identifying geographic regions where the ASI exhibits high sensitivity to global climate change.

B. Previous investigations of the response of air quality to global warming have implicitly incorporated GCM biases into future air quality projections [e.g., 10-15]. However, simulated changes in the exceedences of daily-scale climate thresholds have been found to be highly sensitive to model biases [23,25]. To limit meteorological threshold errors associated with air stagnation sensitivities, we identify and correct biases in the daily-scale atmospheric conditions simulated by the CMIP3 models.

C. Previous investigations of air stagnation conditions and climate-chemistry interactions have been limited to very small model ensembles [e.g., 10-15]. We examine the spread in simulated air stagnation conditions across the multi-GCM CMIP3 ensemble with the intention of providing some insight into the uncertainties in the response of air stagnation to global warming, including implications for climate-chemistry studies based on native climate fields derived from single-GCM experiments.

2. Method

The NCDC ASI is based on daily precipitation, 500-mb winds and near-surface winds. We were able to obtain the necessary daily three-dimensional atmospheric fields for the late-20th century (1981-2000; 20C3M simulation) and late-21st century (2081-2100; SRES-A1B scenario) from 16 of the 25 CMIP3 Atmosphere-Ocean GCMs (AOGCMs) (Table S1) [16]. We refer to these 16 AOGCMs as the CMIP3 ensemble. The horizontal resolution of these AOGCMs ranges from 1.1° latitude [s0] 1.1° longitude to 4.0° [s0] 5.0°, with atmospheric fields provided for either 9 or 17 pressure levels (Table S1).

To determine the influence of climate change on air stagnation frequency, our analysis compares historic (late-20th century) model simulations to future (late-21st century) model simulations using climate model fields that have been bias corrected with an observational standard. Implicit in all such bias correction approaches is the assumption that the structure of model biases identified in historical analyses will remain similar in future projections [26,27]. We use the NCEP/DOE R2 10-meter and 500-millibar wind fields (2.5° [s0] 2.5°) [21] and the Matsuura and Willmott [22] global terrestrial precipitation dataset (1.0° [s0] 1.0°) as our observational standards. We employ the quantile-based bias correction technique developed by Ashfaq et al [23,24] to remove CMIP3 ensemble member biases (see Supplementary data). This correction technique removes errors in the GCM-simulated monthly average magnitude of meteorological variables, but does not correct biases in the simulated response of the variables to climate change, as such corrections would require a priori knowledge of the response of the climate system to enhanced radiative forcing.

We assess air mass stagnation using the NCDC Air Stagnation Index (ASI). This metric gauges the frequency with which atmospheric conditions allow for the accumulation of gaseous and/or particulate pollution. The ASI is based on meteorological thresholds formulated for the conterminous United States by Wang and Angell [19] and is calculated for each individual grid cell. In our study, a given day is considered to meet stagnation criteria when daily mean 500-mb wind speed is less than 13 m s^{-1}, daily mean 10-m wind speed is less than 3.2 m s^{-1}, and daily total precipitation is less than 1.0 mm (i.e., a dry day).

If the value of any of the individual parameters is greater than the respective threshold, the air mass over that grid cell is not considered stagnant. We calculate air stagnation on a daily basis and determine the percentage of days per year that meet the stagnation criteria. We then average these yearly totals across the 20 years of available model data to determine the mean annual late-20th and late-21st century air stagnation occurrences. Similar to the NCDC (but unlike [19]), we place no length requirements on stagnation events, but acknowledge that periods of persistent stagnation may have a different impact than an equal number of intermittently-spaced stagnation days. In this manuscript, we present absolute changes in the ASI and its constituent components to quantify the average departure, in number of days/year, from the baseline to the future period. In addition, we examine relative changes in the ASI, in percentage change in the number of days/year, to highlight areas where stagnation regimes are most sensitive to global warming relative to baseline occurrence (e.g., emergent stagnation hot spots).

3. Results

3.1 Annual Occurrence

Analysis of the late-20th century bias corrected CMIP3 ensemble indicates that on average the conditions for stagnant air are met on 50% of days per year within the subtropical latitudes, with the remainder of the global domain experiencing fewer stagnant days and substantial regional heterogeneity (Figure 1a). (As expected from the bias correction method, the ensemble mean of the bias corrected stagnation frequency is very similar to the reanalysis stagnation frequency (Figure S4).) Projected changes in late-21st century air stagnation are spatially heterogeneous, with increases of up to 12-to-25% relative to the late-20th century occurring over many of the world's industrialized population centers, including those in the eastern United States, Mediterranean Europe, and eastern China (Figure 1b). Substantial increases (>9 days/year) in stagnation occurrence are also projected for portions of Central America, northern South America, southern Africa, central Asia, the Persian Gulf region, and northern India (Figure 1c). Late-21st century decreases in air stagnation frequency are generally of a lower magnitude, with only one region – mid-latitude South America – exhibiting reductions of greater than 9 days/year (Figure 1c).

The magnitude and pattern of projected changes in stagnation frequency result from changes in the individual stagnation components, each of which exhibits a different pattern of response to elevated greenhouse forcing (Figure 2). The magnitude of change in the frequency of days meeting the respective stagnation thresholds is generally below ±16% for each component (Figure 2d-f). The 500-mb wind field indicates zonally consistent alteration of upper level wind speeds, with the greatest relative change occurring in the mid-latitudes, coincident with the mean position of both the northern and southern polar jets (Figure 2a,d). In general, the northern mid-latitudes of the Northern Hemisphere (NH) are projected to have fewer 500-mb stagnation days, whereas increases are projected for the southern mid-latitudes into the northern tropics (Figure 2g). The spatial pattern of change in the 10-meter wind field is more heterogeneous (Figure 2b,e), with the majority of the U.S., non-Scandinavian Europe, and southern Asia exhibiting a 3-to-12 day/year increase in the frequency of stagnant 10-m wind conditions (Figure 2h). Twenty-first century changes in precipitation result in a relative decrease of up to 12% in the occurrence of dry days over the northern high latitudes, across the Horn of Africa, and throughout much of Asia (Figure 2c,f). Most of the remainder of the global domain exhibits increases in dry days, including relative increases of 12-to-24% over the Amazon Basin, the Indonesian archipelago, and across Mediterranean Europe (Figure 2f).

The 16 models that comprise our bias corrected CMIP3 ensemble demonstrate varying levels of agreement in the effects of global warming on the ASI and its individual

components (Figure 3). The inter-model standard deviation of relative change in ASI varies by more than 20% of days/year over some regions of the globe, with pockets of the northeastern U.S., south-central Europe, and the tropics exhibiting the largest spreads (Figure 3a). Inter-model spread in the absolute change of the ASI is generally lower in magnitude in the mid-latitudes than in the tropics, though portions of the southern U.S. (ASI [s1] from 3-9 days/year) and Mediterranean Europe (ASI [s1] from 6-18+ days/year) exhibit spreads of up to 6-9 and 9-12 days/year, respectively (Figure 3e). Of the three stagnation components, the 10-m wind field exhibits the highest inter-model standard deviation of projected relative change (Figure 3c), with spreads of 4-to-12% of days/year over much of Earth's surface (Figure 3c). The inter-model spread of the relative change in both the 500-mb wind and precipitation fields is generally lower, with standard deviations of 0-to-8% of days/year over the majority of the global domain (Figure 3b and d). Of the three components, inter-model spread in absolute change is greatest in the 500-mb wind field, particularly over central Canada, mid-latitude South America, and northern Europe (500-mb [s1]'s from 9-20 days/year), all of which exhibit standard deviations of 15-20 days/year (Figure 3f). The largest inter-model spreads in absolute change in the precipitation and 10-m wind fields exhibit greater spatial heterogeneity (Figure 3g and h), though broad swaths of both northern South America (dry day [s1] from 15-25 days/year) and south-central Europe (dry day [s1] from 15-30 days/year) exhibit spreads of up to 20 days/year in dry day occurrence (Figure 3h).

3.2 Seasonal Occurrence

The creation and accumulation of atmospheric pollutants – including particulate matter, tropospheric ozone, and the precursors of tropospheric ozone – demonstrate varying degrees of dependency on seasonal meteorological conditions [10-12,17]. For example, particulate matter is readily scavenged from the atmosphere via precipitation, whereas tropospheric ozone and its precursors are only minimally affected by precipitation due to their low solubilities [9]. The seasonal distribution of precipitation therefore has a larger influence on the accumulation of particulate matter in the atmosphere than on ozone concentrations. Conversely, the production and concentration of tropospheric ozone and its precursors is highly dependent on seasonal temperatures and the distribution of sunlight and vegetation, and therefore typically peaks in the summer months, while the concentration of particulate matter demonstrates no specific relationship with available sunlight [9].

Given these seasonal nuances, we examine changes in late-21st century seasonal stagnation occurrence, with emphasis on three illustrative regions that exhibit both high population density and substantial projected relative increases in annual air stagnation frequency: the eastern United States, Mediterranean Europe, and eastern China. We also examine projected changes in absolute seasonal temperatures, which could amplify pollutant concentration changes brought about by altered late-21st century air stagnation occurrence [28-30]. Regional values are determined by calculating the average seasonal stagnation occurrence (or stagnation component occurrence) within each grid cell and then weight-area averaging all grid cells within the chosen domain (a process that dampens the magnitude of individual grid cell variability). Domain boundaries are outlined by black rectangles in Figure 1b. To quantify the distribution of CMIP3 projections, we examine the minimum, maximum and mean of the GCM values, along with the range between the first (Q1) and third (Q3) quartiles (Figure 4; for the corresponding absolute change plot see Figure S1).

3.2.1. Eastern United States—Stagnation days increase over the eastern United States in all four seasons in the late-21st century (Figure 4a). The autumn and winter seasons (SON & DJF) exhibit the greatest relative increases in seasonal stagnation occurrence (~20%), while the summer season (JJA) exhibits the smallest (~12%). In absolute terms, the largest

increase in stagnation occurrence occurs in the summer and fall seasons, with ~2 additional days/season projected (Figure S1a). The relative increases in both the autumn and winter seasons are largely attributable to increasing occurrence of light 500-mb wind speeds. In contrast, the relative summer increase results from minor increases (~2-to-7%) in each individual stagnation component (fewer wet days, more days with light 10-m winds, and more days with light 500-mb winds). Summer exhibits the greatest model agreement in relative change in ASI, while spring and winter exhibit the greatest Q1-to-Q3 spreads, and all four seasons exhibit substantial range between the maximum and minimum change (Figure 4a). Of the individual components, summer dry days, autumn 500-mb winds, and winter 500-mb winds exhibit the greatest Q1-to-Q3 spreads. Temperatures in the Eastern United States are projected to increase in each late-21st century season, with the greatest absolute increases projected to occur in the autumn and summer (although these seasons also exhibit the greatest Q1-to-Q3 spreads).

3.2.2. Mediterranean Europe—Stagnation days are projected to increase over Mediterranean Europe in all four seasons in the late-21st century, with the autumn (~18%) and summer (~15%) seasons exhibiting the largest relative ensemble mean increases (Figure 4b). Absolute increases in stagnation occurrence are also largest in the autumn and summer seasons, with ~2.5-3 additional stagnation days/season projected (Figure S1b). Relative increases are largely attributable to decreasing occurrence of wet days and increasing occurrence of light 500-mb winds. The ~13% relative increase in spring (MAM) stagnation days is mostly attributable to an ~13% increase in dry days, although this gain is tempered by a reduction in the number of days with light 500-mb winds. Winter exhibits the narrowest max-to-min ASI spread, though Q1-to-Q3 spreads are substantial in all seasons. Of the individual components, the Q1-to-Q3 inter-model spreads in the dry day and 10-m wind fields are greatest in DJF, which is the Mediterranean's winter wet season, while the projected relative change in 500-mb winds exhibits similar Q1-to-Q3 spreads for each season (Figure 4b). Temperatures in Mediterranean Europe are projected to increase in all seasons in all ensemble members, with the summer season exhibiting both the greatest absolute increase and the greatest Q1-to-Q3 spread.

3.2.3. Eastern China (& the Korean Peninsula)—Stagnation days over Eastern China and the Korean Peninsula are expected to increase in each season during the late-21st century. The greatest relative increase in stagnation frequency is projected for the autumn season, with ~17% more days per season meeting stagnation criteria, largely attributable to an increase in the occurrence of light 500-mb and 10-m winds (Figure 4c). In absolute terms the autumn season also exhibits the largest increase, with ~2 additional days/season projected (Figure S1c). The relative change in summer season stagnation occurrence is the lowest of the three regions, exhibiting an ~7% increase in stagnation days, with minor positive contributions from each stagnation component. Summer exhibits the greatest model agreement, while winter exhibits the largest Q1-to-Q3 spread due to substantial spread in the 500-mb wind field. With the exception of the winter 500-mb wind field, Q1-to-Q3 spreads of individual components are small relative to the other regions, suggesting greater ensemble agreement (Figure 4c). In contrast with the other two regions, seasonal temperatures in Eastern China exhibit the largest change during the winter season. The four seasons exhibit approximately equal Q1-to-Q3 spreads in temperature change, though the max-to-min temperature spread is larger in winter than in the other seasons.

4. Discussion and Conclusions

Impact metrics such as the ASI offer an important perspective on the influence of global warming on the dynamics of the climate system. For example, our analysis finds that the projected autumn and winter increases in stagnation days over eastern China and the eastern

United States are largely caused by changes in the 500-mb wind field (Figure 4a,c). These changes are consistent with findings from previous studies that suggest global warming will lead to a northward shift of the Northern Hemisphere polar jet stream and/or fewer southward excursions of the storm track due to a reduction in cyclogenesis [14,31,32]. Likewise, our analysis suggests that the projected increases in stagnation days over Mediterranean Europe are largely caused by increases in the occurrence of precipitation-free days (Figure 4b). These changes in dry day frequency agree with the more general climate model projection of altered 21st century precipitation patterns and increased aridity over the region [e.g., 16,33]. Changes in individual stagnation components can work both for and against increases/decreases in regional stagnation occurrence. For instance, substantial increases in tropical dry day occurrence are offset by projected decreases in stagnation occurrence in the 500-mb wind and 10-m wind fields. Similarly, projected decreases in dry day occurrence in the NH high-latitudes are countered by increases in the occurrence of 500-mb wind field stagnation (Figure 2d-i).

In our application of the ASI it is important to consider that it is a synoptic-scale metric that does not explicitly incorporate all of the meteorological factors known to influence air quality (e.g., relative humidity, temperature, etc. [cf. 9]). Further, the ASI does not explicitly account for site-specific factors such as orographic boundaries or marine inversions. As a consequence of this synoptic-scale applicability, ASI component threshold sensitivities may be locally variable, and meteorological factors in addition to, or exclusive of, air stagnation, may play a substantial role in determining air quality within local environments. Despite these considerations, the ASI metric and its component thresholds were formulated based on observational analyses of stagnation events across the contiguous U.S. [19], indicating that its formulation is broadly applicable throughout diverse synoptic environments and that its application within the confines of relatively coarse resolution GCMs is appropriate.

A primary implication of our analysis of the bias corrected CMIP3 ensemble is the potential for continued 21st century global warming to alter the meteorological conditions that facilitate the accumulation of near-surface ozone and particulate matter. Projected changes in stagnation occurrence, when weighted with year 2000 gridded population counts [34], demonstrate that populations within the eastern United States, Central America, southern Europe, northern India, and eastern China, are particularly susceptible to air quality impacts that result from altered stagnation regimes, though this analysis does not account for population dynamics or changing emissions over the coming century (Figure S10). The ensemble mean of the bias corrected CMIP3 realizations suggests that many industrial population centers, including Mexico City, Atlanta, New York City, Rome, New Delhi, Shanghai, and Beijing, and the regions that surround them, could experience 12-to-25% relative increases (3-18+ days/year) in stagnant atmospheric conditions, thereby exacerbating pre-existing air quality issues and increasing the likelihood that air quality will be degraded more frequently relative to the late-20th century (Figure 1). Our analysis focuses on three of these industrialized high-population regions and finds that the synoptic conditions over these areas are particularly sensitive to increased radiative forcing (Figure 1b,c). Compounding the effects of increased stagnation, projected seasonal regional temperature increases (Figure 4) have the potential to (a) amplify pollutant concentrations due to increases in chemical reaction rates and/or (b) make non-summer stagnation changes more relevant, should temperatures in non-summer seasons increase sufficiently to exceed critical chemical reaction thresholds [28-30]. Based on these projections, if future Clean Air objectives are to be met [e.g. 6-8], more stringent emission control measures may be required in order to offset the effects of global warming on stagnation frequency (with the caveat that we have not explored potential changes in atmospheric chemistry, which could also influence the response of air quality [e.g., 11,28-30]).

In an effort to determine the response of air quality to enhanced radiative forcing the majority of air quality assessments to date, have relied on native atmospheric fields from single GCMs to drive chemical transport and/or nested climate models [e.g., 10-15]. Our results have important implications for these approaches. For example, we find substantial variation in the ability of individual CMIP3 GCMs to accurately simulate late-20th century stagnation conditions (Figure S2). Indeed, each CMIP3 ensemble member exhibits ASI biases in excess of ±25% of days/year over large portions of the global domain (Figure S3), suggesting deficiencies in each GCM's ability to simulate at least some of the atmospheric conditions that contribute to air stagnation. Bias correction improves each model's ability to replicate the observed frequency of late-20th century stagnation (Figure S4), reducing ensemble member ASI biases substantially below ±25% of days/year in almost all regions (Figure S5). Our results indicate that of the three constituent air stagnation components, bias correction is most effective at removing the errors in the 500-mb wind field and least effective at removing errors in the precipitation field (Figures S6-8).

Because the monthly-mean of each stagnation component is, by definition, identical within each bias corrected ensemble member over the late-20th century period, differences in the late-20th century stagnation values between bias corrected ensemble members result from differences in the daily-scale variability simulated in the individual climate models (Figure S4-S5). It is the combination of this daily-scale variability and differences in each model's simulated response to global warming that produces the inter-model spread in the bias corrected stagnation projections (Figures 3 and 4). Although the bias correction reduces the spread in the CMIP3 ensemble (Figure S2, S4), the fact that inter-model differences in the projected change in air stagnation frequency persist after bias correction (Figure 3-4) has important implications for other efforts to assess the impacts of climate change on air quality. In particular, assessments that utilize different GCMs for explicitly calculating changes in air quality (through either coupled or off-line atmospheric chemistry modeling) may provide substantially different projections of future air quality, simply because of the inter-GCM differences in atmospheric stagnation (Figures 4 and S9). To improve future assessments of air quality, our analysis suggests that using bias corrected GCM fields as inputs in chemical transport models and nested climate models would likely yield an improved representation of atmospheric conditions, while the use of a multi-model ensemble of climate-chemistry simulations would more realistically capture the range of uncertainties in the simulated response of the atmosphere to increased radiative forcing [35].

Although we have not explicitly assessed the response of air quality to changes in atmospheric chemistry, our analysis of the atmospheric conditions simulated by the CMIP3 ensemble suggests that global warming could alter air quality over a number of regions through changes in the frequency of air stagnation events. These projected changes in air stagnation occurrence could be expected to have the greatest impact over areas where increasing stagnation co-occurs with high population densities and high surface emission rates. Our multi-model analysis identifies a number of such regions, including the eastern United States, Mediterranean Europe, and eastern China. Given the current impacts of poor air quality episodes, the projected increases in air stagnation frequency of 12-to-25% could be expected to exacerbate the socio-economic burdens faced by the citizens and governments of these regions [1-3]. Although additional atmospheric chemistry modeling is required to explicitly calculate air quality impacts, our results suggest that changes in the atmospheric circulation caused by anthropogenic greenhouse forcing could increase the risk of poor air quality by increasing the frequency of air stagnation events over highly populated, highly industrialized areas.

Supplementary Material

Refer to Web version on PubMed Central for supplementary material.

Acknowledgments

NCEP/DOE R2 data provided by the NOAA/OAR/ESRL PSD, Boulder, Colorado, USA, from their website at http://www.esrl.noaa.gov/psd/. We acknowledge the World Climate Research Programme's Working Group on Coupled Modelling, the climate modeling groups, and DOE's PCMDI for making the CMIP3 data available. Our work was supported by the DOE Grant No. DE-SC005171, along with supplementary support from NIH award 1R01AI090159-01.

References

[1]. Matus K, Nam K-M, Selin NE, Lamsal LN, Reilly JM, Paltsev S. Health damages from air pollution in China. Glob. Environ. Chan. 2012; 22:55–66.

[2]. European Environment Agency. Revealing the costs of air pollution from industrial facilities in Europe. European Union; Copenhagen, Denmark: 2011.

[3]. Muller NZ, Mendelsohn R, Nordhaus W. Environmental accounting for pollution in the United States economy. Amer. Ec. Re.v. 2011; 101:1649–75.

[4]. www.airqualitynow.eu

[5]. www.airnow.gov

[6]. European Commission. The Clean Air For Europe Programme (CAFE): Toward a Thematic Strategy for Air Quality. European Union; 2001.

[7]. Clean Air Act Amendments of 1990. United States of America; 1990. Public Law 101-549

[8]. Standing Committee of the National People's Congress. Law of the People's Republic of China on the Prevention and Control of Atmospheric Pollution. People's Republic of China; 2000.

[9]. Jacob DJ, Winner DA. Effect of climate change on air quality. Atmos. Environ. 2009; 43:51–63.

[10]. Leung LR, Gustafson WI. Potential regional climate change and implications to U.S. air quality. Geophys. Res. Lett. 2005; 32:L16711.

[11]. Racherla PN, Adams PJ. U.S. ozone air quality under changing climate and anthropogenic emissions. Environ. Sci. Technol. 2009; 43:571–7. [PubMed: 19244985]

[12]. Tai APK, Mickley LJ, Jacob DJ. Correlations between fine particulate matter ($PM_{2.5}$) and meteorological variables in the United States: Implications for the sensitivity of $PM_{2.5}$ to climate change. Atmos. Envir. 2010; 44:3976–84.

[13]. Tai APK, Mickley LJ, Jacob DJ, Leibensperger EM, Zhang L, Fisher JA, Pye HOT. Meteorological modes of variability for fine particulate matter ($PM_{2.5}$) air quality in the United States: implications for $PM_{2.5}$ sensitivity to climate change. Atmos. Chem. and Phys. Disc. 2011; 11:31031–66.

[14]. Mickley LJ, Jacob DJ, Field BD, Rind D. Effects of future climate change on regional air quality episodes in the United States. Geophys. Res. Lett. 2004; 31:L24103.

[15]. Leibensperger EM, Mickley LJ, Jacob DJ. Sensitivity of US air quality to mid-latitude cyclone frequency and implications of 1980-2006 climate change. Atmos. Chem. Phys. 2008; 8:7075–86.

[16]. Meehl, GA., et al. IPCC Climate Change 2007: The Physical Science Basis. Soloman, S., et al., editors. Cambridge Univ. Press; 2007.

[17]. TOR-2 2003 Tropospheric Ozone Research, EUROTRAC-2 Subproject Final Report. ISS GSF-National Research Center for Environment and Health; Munich, Germany:

[18]. Korshover J, Angell JK. A review of air-stagnation cases in the eastern United States during 1981-Annual Summary. Mon. Weather Rev. 1982; 110(10):1515–18.

[19]. Wang, JXL.; Angell, JK. Air Stagnation Climatology for the United States (1948-1998). 1999. NOAA/Air Resources Laboratory ATLAS, No.1

[20]. www.ncdc.noaa.gov/societal-impacts/air-stagnation

[21]. Kanamitsu M, Ebisuzaki W, Woollen J, Yang S-K, Hnilo JJ, Fiorino M, Potter GL. NCEP-DOE AMIP-II Reanalysis (R-2). Bul. Atmos. Met. Soc. 2002; 83:1631–43.

[22]. Matsuura, K.; Willmot, CJ. Terrestrial precipitation: 1900-2008 Gridded Monthly Time Series (Version 2.01). 2009. http://climate.geog.udel.edu/~climate/

[23]. Ashfaq M, Bowling, Cherkauer K, Pal JS, Diffenbaugh NS. Influence of climate model biases and daily-scale temperature and precipitation events on hydrological impact assessments: A case study of the United States. J. Geophys. Res. 2010a; 115:D14116.

[24]. Ashfaq M, Skinner CB, Diffenbaugh NS. Influence of SST biases on future climate change projections. Clim. Dyn. 2010b doi:10.1007/s00382-010-0875-2.

[25]. Diffenbaugh NS, Scherer M. Using climate impacts indicators to evaluate climate model ensembles: temperature stability of premium winegrape cultivation in the United States. Clim. Dyn. 2012 doi:10.1007/s00382-012-1377-1.

[26]. Wood WW, Maurer EP, Kumar A, Lettenmaier DP. Long-range experimental hydrologic forecasting for the eastern United States. J. Geophys. Res. 2002; 107(D20):4429.

[27]. Wood WW, Leung LR, Sridhar V, Letternmaier DP. Hydrological implication of dynamical and statistical approaches to downscaling climate model outputs. Climatic Change. 2004; 62:189–216.

[28]. Jacob DJ, Logan JA, Gardner GM, Yevich RM, Spivakovsky CM, Wofsy SC. Factors regulating ozone over the United States and its export to the global atmosphere. J. Geophys. Res. 1993; 98:817–26.

[29]. Sillman S, Samson PJ. The impact of temperature on oxidant formation in urban, polluted rural, and remote environments. J. Geophys. Res. 1995; 113:D07307.

[30]. Stenier AL, Davis AJ, Sillman S, Owen RC, Michalak AM, Fiore AM. Observed suppression of ozone formation at extrememly high temperatures due to chemical and biophysical feedbacks. Proc. Nat. Acad. Sci. USA. 2010; 107:19685–90. [PubMed: 21041679]

[31]. Yin JH. A consistent poleward shift of the storm tracks in simulations of 21st century climate. Geophys. Res. Lett. 2005; 32:L18701.

[32]. Trapp RJ, Diffenbaugh NS, Gluhovsky A. Projected trends in severe extratropical thunderstorm forcing. Geophys. Res. Lett. 2009; 36:L01703.

[33]. Giorgi F. Climate change hot-spots. Geophys. Res. Lett. 2006; 33:L08707.

[34]. Center for International Earth Science Information Network/Colombia University. United Nations Food and Agriculture Programme. Centro Internacional de Agricultura Tropical 2005. Gridded Population of the World Version 3: Population Count Grid. NASA Socioeconomic Data and Applications Center; Palisades, New York:

[35]. Collins M. Ensembles and probabilities: a new era in the prediction of climate change. Phil. Trans. R. Soc. A. 2007; 365:1957–70. [PubMed: 17569649]

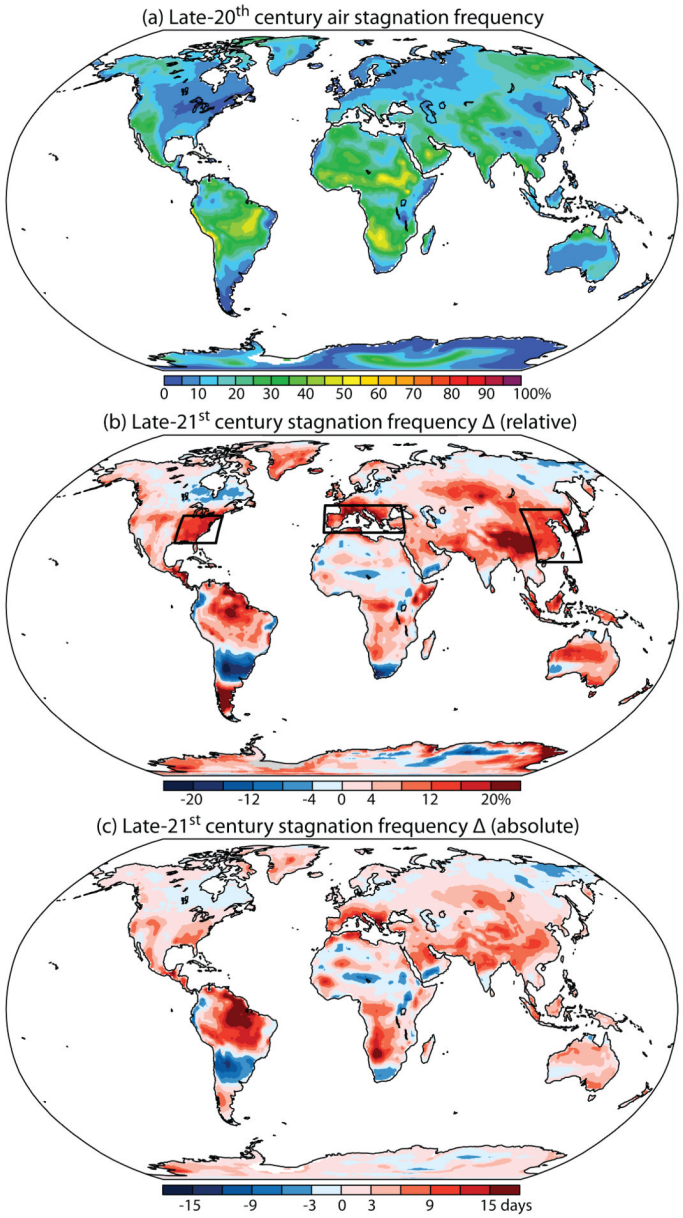

Figure 1.

Historic and future changes in simulated ensemble mean annual air stagnation occurrence. (a) Late-20th century bias corrected air stagnation occurrence (percentage of days per year that meet the NCDC ASI criteria). (b) Relative change in bias corrected stagnation occurrence from the late-20th to late-21st century (percent change of days/year). (c) Absolute change in bias corrected stagnation occurrence from the late-20th to late-21st century (days/year). For plots b and c weighted by population, see Figure S10.

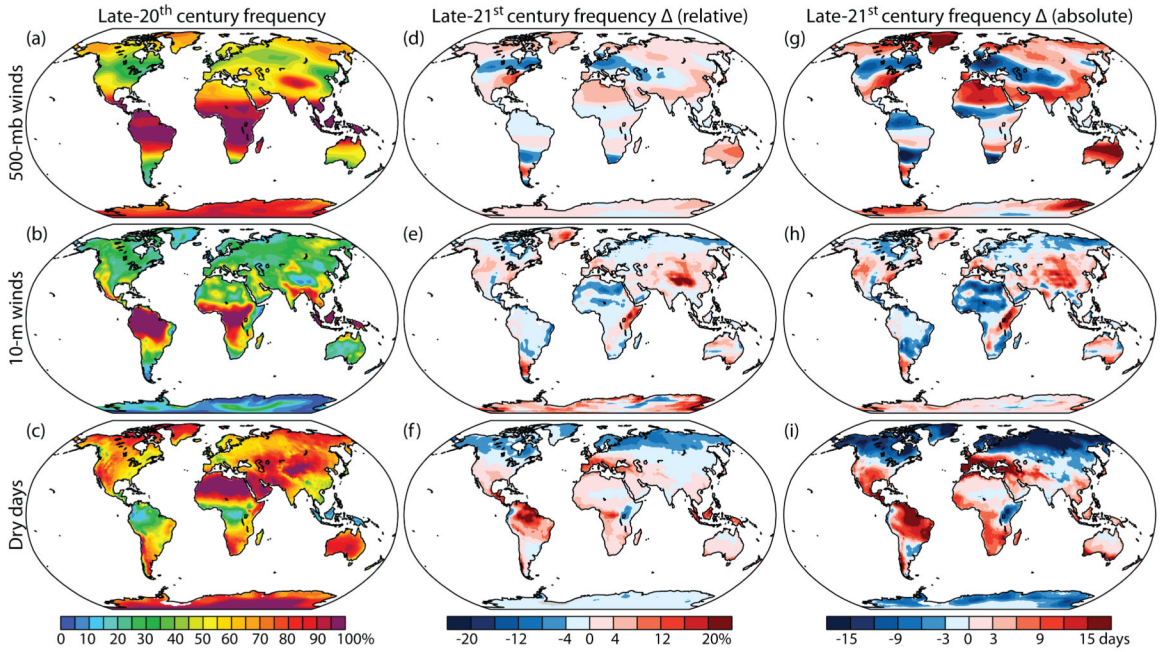

Figure 2.

Historic and future changes in simulated ensemble mean annual air stagnation components. (a-c) Late-20th century bias corrected stagnation components (percent of days/year). (d-f) Relative change of bias corrected air stagnation components, late-20th to late-21st century (percent change of days/year). (g-i) Absolute change of bias corrected air stagnation components, late-20th to late-21st century (days/year). Top row (a,d,g) is 500-mb winds, middle row (b,e,h) is 10-m winds, and bottom row (c,f,i) is dry day occurrence.

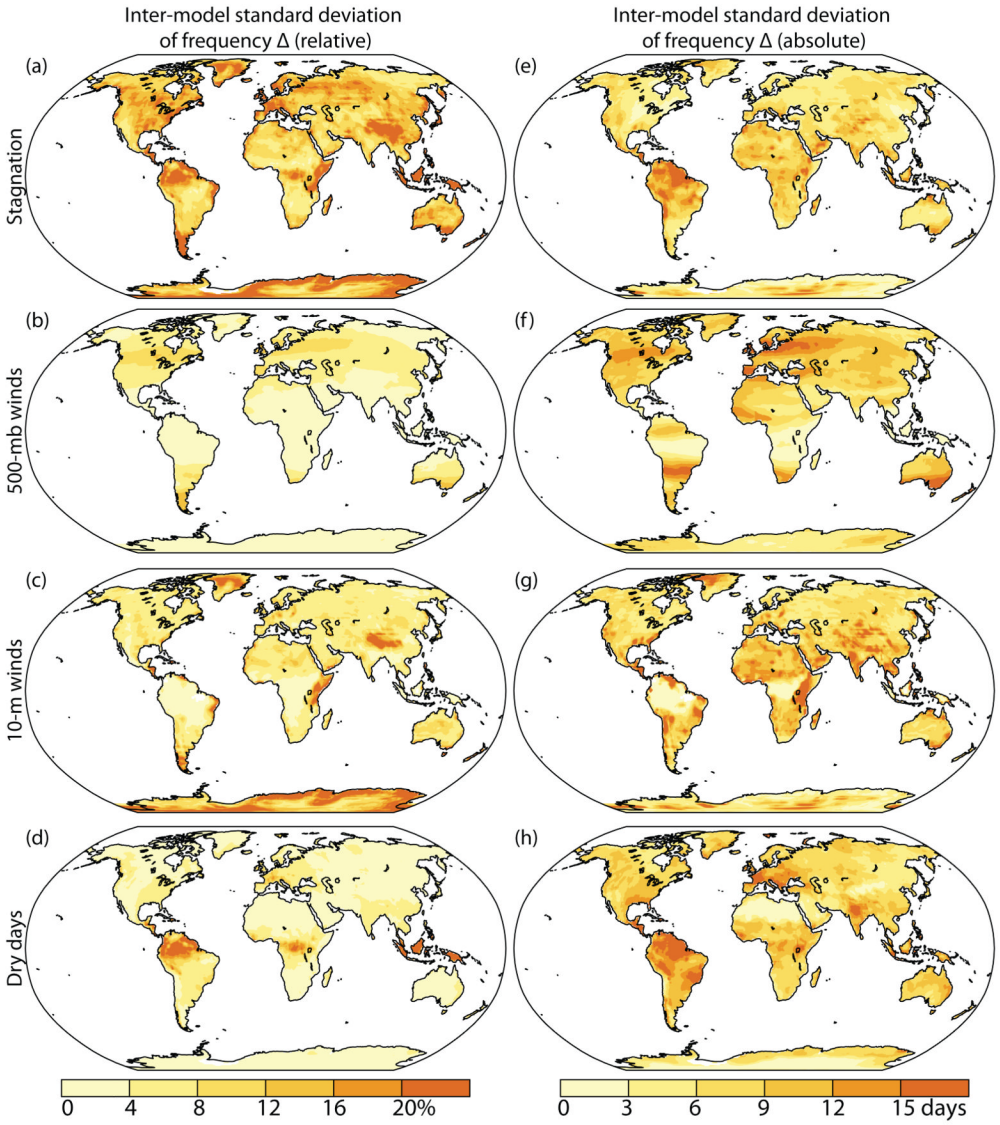

Figure 3.

Inter-model spread of the response of air stagnation and its components to global warming (late-20th to late-21st century). (a-d) Standard deviation of the relative change (percent of days/year) and (e-h) absolute change (days/year) of (a,e) air stagnation occurrence, (b,f) 500-mb winds, (c,g) 10-m winds, and (d,h) dry day occurrence across the CMIP3 ensemble.

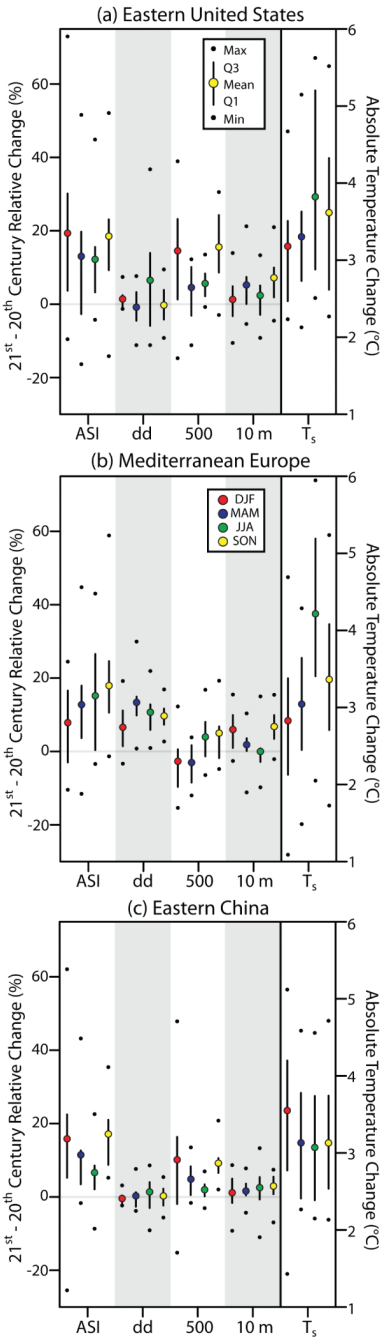

Figure 4.

Relative seasonal stagnation changes of the ensemble members, for (a) the Eastern United States, (b) Mediterranean Europe, and (c) Eastern China and the Korean Peninsula. Y-axis values are the percent change in days per season. Regional values are determined by calculating the average seasonal stagnation occurrence (or stagnation component occurrence) within each grid cell and then weight-area averaging all grid cells within the chosen domain. Domain boundaries are outlined by black rectangles in Figure 1b. Abbreviations: *ASI* – Air Stagnation Index, *dd* – dry days, *500* – 500-mb winds, *10 m* – 10 m winds, and T_S – surface temperature. Statistical abbreviations found in inset (a) are in reference to the CMIP3 ensemble members: *Max* – Maximum simulated value, *Min* –

Minimum simulated value, *Q1* – First quartile, *Q3* – Third quartile. Seasons are color-coded and labeled in inset (b). For the corresponding plot in absolute change, see Figure S1.